REPORT
4/2018
ISBN 978-82-7492-403-1
ISSN 2535-3004

# SCIENTIFIC ASSESSMENT OF TSCV RETRIEVAL FROM STEREO-SAR – A CRITICAL REVIEW

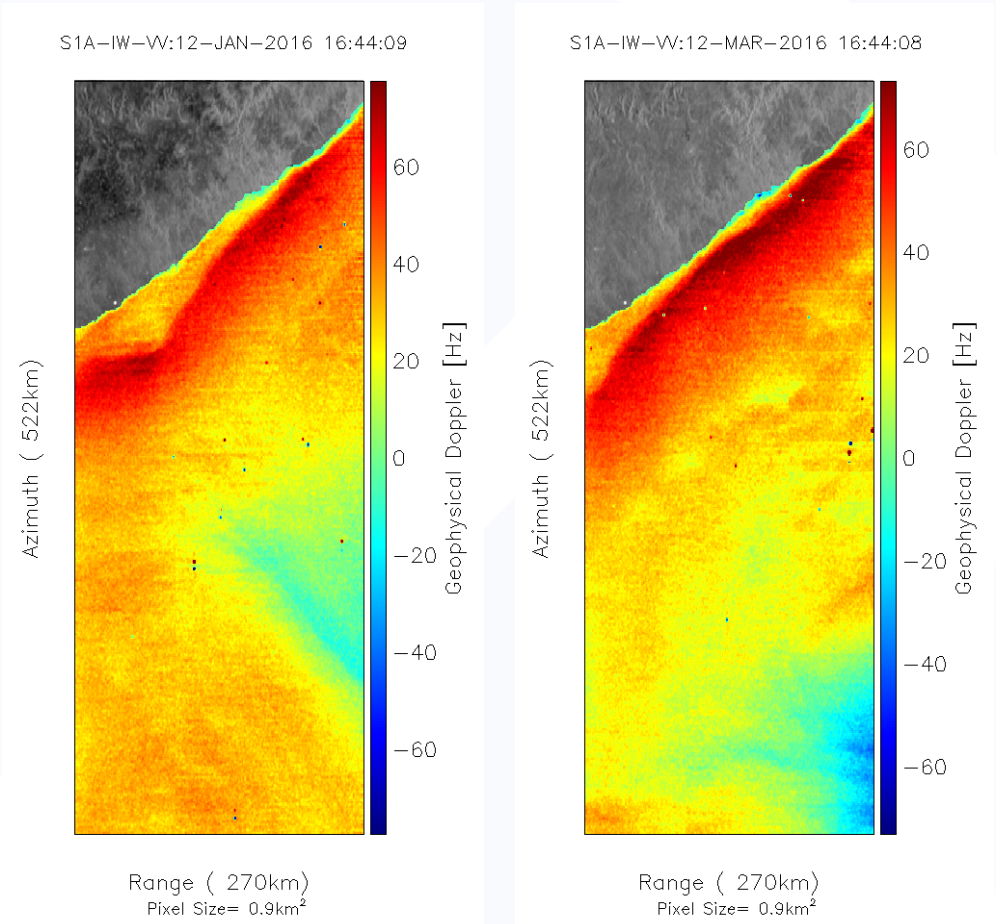


Editor: Harald Johnsen

P.O. BOX 6434, TROMSØ SCIENCE PARK
N-9294 TROMSØ, NORWAY
TEL: +47 77 62 94 00, FAX: +47 77 62 94 01
post@norut.no
www.norut.no

norut
NORTHERN RESEARCH INSTITUTE

**Project name: SATRoSS** **Project No.: 712**

Contractor (s): Contract ref.: 4000121959/17/NL/AI

Document No.: 4/2018 Document Type: Report Status: Open

ISBN: 978-82-7492-403-1 ISSN: 2535-3004 No. Pages: 28

Project manager: Harald Johnsen Dato: 2018-03-16

Author (s): H. Johnsen (Norut), F. Nouguier (Ifremer), B. Chapron (Ifremer), F. Collard (OceanDataLab), P.L.Dekker (TU Delft)

# Title: Scientific Assessment of TSCV Retrievals from Stereo-SAR – A critical Review

Resymé / Summary:

A critical review of the mission requirements [R-3] is described. Emphasis is put on limitations and requirements put on the geophysical models for the baseline system parameters and observation geometry in order to meet the user requirements.

A review of forward models (mono- and bistatic) for NRCS, DCA and SAR wave spectra is provided, and necessary improvement and extension to be implemented in Task 2 are defined. A similar approach is applied to retrieval schemes to be implemented in Task 3. Of particular importance is the necessity of a synergetic approach to the retrieval of wind, wave (partly) and current fields. Simulations show that very accurate estimates of local wind vector and wind sea waveheight are needed in order to meet the requirement of an accuracy of retrieved surface current speed of $\leq 0.3\ m/s$.

The baseline observation concept to consider is shown in Figure 1.

Keywords: SAR, Sentinel 1, bi-static, ocean surface current, ocean surface wind

Notes:

Publisher: Norut

# Content:

**Abbreviations:**

| | | |
|---|---|---|
| ATI | - | Along Track Interferometry |
| ADCP | - | Acoustic Doppler Current Profiler |
| CS | - | Companion Satellite |
| DC | - | Doppler Centroid |
| DCA | - | Doppler Centroid Anomaly |
| ENL | - | Equivalent Number of Looks |
| LBB | - | Long Baseline Bistatic |
| LBS | - | Long Baseline Stereostatic |
| NRCS | - | Normalized Radar Cross Section |
| NESZ | - | Noise Equivalent Sigma Zero |
| OSC | - | Ocean Surface Current |
| RAR | - | Real Aperture Radar |
| S1 | - | Sentinel 1 |
| S2 | - | Sentinel 2 |
| SAR | - | Synthetic Aperture Radar |
| TSCV | - | Total Surface Current Vector |

*Reference Documents:*

R-1 Scientific Assessment of TSCV Retrievals from Stereo-SAR (SATRoSS) - Statement of Work, ITT AO/1-8875/17/NL/AI, EOP-SM/3099, Issue 1, 27/02/2017
R-2 Fois F., "S1+CS Selected Concept Performance Analysis Report", S1CS.ASU.SY.PR.0000X, Issue 2.0, 2016
R-3 S1+CS Mission Requirements Document, S1CS.ASU.SY.RP.00001, Issue 2.0, August 2016
R-4 S1+CS Mission System Design and Analysis Report, S1CS.ASU.SY.RP.0006, Issue 2.1, January 2017

*Applicable Documents:*

A-1 Durand, M., Lee-Lueng Fu, D.P. Lettenmaier, D.E. Alsdorf, E. Rodriguez; D. Esteban-Fernandez, (2010), "The Surface Water and Ocean Topography Mission: Observing Terrestrial Surface Water and Oceanic Submesoscale Eddies," Proceedings of the IEEE , vol.98, no.5, pp.766,779.
A-2 Gommenginger, C., B. Chapron, J. Marquez, B. Richards, M. Caparrini, G. Burbidge, D. Cotton, Adrien C.H. Martin (2014), "Wavemill: a new mission for high-resolution mapping of total ocean surface current vectors,"EUSAR 2014; 10th European Conference on Synthetic Aperture Radar; Proceedings of , vol., no., pp.1,4
A-3 Caubet E., Ardhuin F., Chapron B., Nouguier F., Tison C., Lalaurie J.C., Thiry N., Richard J. Phalippou L.. "Preliminary design and performance of the SKIM Ka-band conical scanning radar", Proceedings of ARSI2017, https://www.researchgate.net/publication/319744704

A-4 Donlon C.,(2013), "ESA Data User Element (DUE) GlobCurrent User Requirement Document (URD)", ESA report EOP-SM/2451/CD-cd, 2013. http://web.nersc.no/globcurrent/

A-5 Sperrevik, A.K., Röhrs, J., Christensen, K.H. (2017): Impact of data assimilation on Eulerian versus Lagrangian estimates of upper ocean transport. J. Geophys. Res. Oceans,122, doi: 10.1002/2016JC012640.

A-6 Røhrs, J., and K. H. Christensen (2015), Drift in the uppermost part of the ocean, Geophys. Res. Lett., 42, doi:10.1002/2015GL066733.

A-7 Breivik, Ø., Ø. Sætra (2001), Real time assimilation of HF radar currents into a coastal ocean model, J. of Marine Systems 28 (2001) 161-182

A-8 Dagestad K.F., J. Röhrs, Ø. Breivik, B. Ådlandsvik, "OpenDrift v1.0: a generic framework for trajectory modeling, https://doi.org/10.5194/gmd-2017-205 (2017)

A-9 Jones C.E., K.F.Dagestad, Ø.Breivik, B. Holt, J. Röhrs, K.H. Christensen, M. Espeseth, C. Brekke, S. Skrunes (2016), Measurement and modeling of oil slick transport, J. Geo.Res. Ocean, DOI 10.1002/2016JCO12113

A-10 Chapron B., F. Collard, F. Ardhuin (2005), "Direct measurements of ocean surface velocity from space: Interpretation and validation", J. Geophysical Research, Vol. 110, No. C7, pp. 10.1029, 2005

A-11 J. A. Johannessen, B. Chapron, F. Collard, V. Kudryavtsev, A. Mouche, D. Akimov, K. F. Dagestad, Direct ocean surface velocity measurements from space: Improved quantitative interpretation of Envisat ASAR observations, Geophysical Research Letters, Vol. 5, DOI:10.1029/2008GL035709, 2008

A-12 Johnsen H., Nilsen V. , Engen G., Mouche A., Collard F. (2016), "Ocean Doppler anomaly and ocean surface current from Sentinel 1 TOPS data", Proceedings IGARSS2016, 10-15 July, Beijing, China

A-13 Suchandt S., A. Lehmann, H. Runge (2014), Analysis of ocean surface current with TanDEM-X ATI: A case study in the Baltic Sea, Proceedings IGARSS2014, 13-18 July, Quebec City, Canada

A-14 Romeiser, R. (2015). Surface current measurements by spaceborne along-track inSAR - terraSAR-X, tanDEM-X, and future systems. In 2015 IEEE/OES 11th Current, Waves and Turbulence Measurement, CWTM 2015 [7098097] Institute of Electrical and Electronics Engineers Inc.. DOI: 10.1109/CWTM.2015.7098097

A-15 Elfouhaily T., B. Chapron, K. Katsaros, D. Vandemark (1997), A unified directional spectrum for long and short wind-driven waves, J. Geophys. Res., Vol.102, no.C7, pp.15781-15796, 1997

A-16 Collard, F., A. Mouche, B. Chapron, C. Danilo, and J. A. Johannessen (2008), Routine high resolution observation of selected major surface currents from space, paper presented at Workshop SEASAR 2008, Eur. Space Agency, Frascati, Italy.

A-17 Rouault, M. J., A. Mouche, F. Collard, J. A. Johannessen, and B. Chapron (2010), Mapping the Agulhas Current from space: An assessment of ASAR surface current velocities,J. Geophys. Res., 115, C10026, doi:10.1029/2009JC006050

A-18 Nouguier Frederic, Chapron Bertrand, Alexis Mouche (2017). Asymptotic methods for microwave scattering, IEEE Remote Sensing Code Library, DOI:10.21982/M8S62C

A-19 Engen G., Pedersen I. F., Johnsen H., Elfouhaily T., "Curvature Effects in Ocean Surface Scattering", IEEE Trans. on Antennas and Propagation, Vol.54, No.5, May 2006

A-20 F. Said, H. Johnsen, Frédéric Nouguier, Bertrand Chapron, and Geir Engen, "Onto a skewness approach to the generalized curvature ocean surface scattering model", *IEEE Trans. Geoscience and Remote Sensing*, ISSN: 1558-0644, DOI 10.1109/TGRS.2017.2715986, 2017

A-21 Johnsen H., Engen G., Guilles G., "Sea surface polarization ratio from Envisat ASAR AP Data", IEEE Transactions on Geoscience and Remote Sensing, Volume 46, Issue 11, Part 1, Nov. 2008 Page(s):3637 – 3646. Digital Object Identifier 10.1109/TGRS.2008.2001061

A-22 Faozi S., H. Johnsen, Bertrand Chapron, and Geir Engen, "An ocean wind Doppler model based on the generalized curvature ocean surface scattering model", IEEE Trans. Geoscience and Remote Sensing, Vol.53, No.12, DOI 10.1109/TGRS.2015.2445057, Dec 2015

A-23 Pedersen F. I., Engen G., Johnsen H., "Polarization Dependency in Doppler Frequency Shift and its Application to Envisat ASAR Alt-Pol Data", Proc. ERS/Envisat Symposium, 6-10 Sept. 2004, Salzburg
A-24 Faozi S., H. Johnsen, "Ocean surface wind retrieval from co-polarized SAR data using the polarization residual Doppler frequency", IEEE Transactions on Geoscience and Remote Sensing, DOI. 10.1109/TGRS.2013.2278550, July 2014
A-25 V. Kudryavtsev, D. Hauser, G. Caudal, and B. Chapron, "A semiempirical model of the normalized radar cross-section of the sea surface 1. Background model," *J. Geophys. Res.*, vol. 108, no. C3, p. 8054, 2003. DOI:10.1029/2001JC001003.
A-26 C. Cox and W. Munk, "Measurement of the roughness of the sea surface from photographs of the sun's glitter," J. Opt. Soc. Am., vol. 44, no. 11, pp. 838–850, Nov 1954. Available: http://www.opticsinfobase.org/abstract.cfm?URI=josa-44-11-838
A-27 G. Engen, H. Johnsen; SAR-Ocean Wave Inversion Using Image Cross Spectra, IEEE Transc. on Geo. Science and Remote Sensing, Vol. 33, No. 4, pp.1047-1056, 1995
A-28 Kræmer T., H. Johnsen, C. Brekke, G.Engen, "Comparing SAR based short time-lag cross-correlation and Doppler sea ice drift velocities ", *IEEE Trans. Geoscience and Remote Sensing, Volume: 56 Issue: 3, ISSN: 1558-0644, DOI: 10.1109/TGRS.2017.2769222, 2017*

# 1. Introduction

One or two passive follower to the Sentinel 1 missions operating in ATI, LBB or LBS modes is a promising concept for measuring ocean surface current from space. The baseline observation concept is shown in Figure 1. This technical note (TN1) addresses the scientific challenges and describes the necessary geophysical forward and retrieval models needed to move the concept from SRL4 to SRL5. Computational efficient geophysical forward models (GMF) (mono- and bistatic) are described with corresponding retrieval models for TSCV field. The unique advantage of the S1+CS to measure simultaneously the surface wind vector, wave field (partly) and DCA is utilized in the retrieval scheme to properly compensate the measured DCA for sea state bias.

The forward and retrieval simulation tools are used to build a performance model for the S1+CS system. The performance model and test scenarios are outlined in the TN2. The performance of S1+CS for TSCV measurements is not only dependent on the system characteristics (TAR, NESZ, ENL,..), but also highly dependent on the ocean surface conditions. Environmental parameter ranges cover both the requirements set by the user community for the OSC field (accuracy, resolution, dynamic range) as well as realistic ranges for expected ocean surface conditions (wave height, wind speed, surface current). An end-to-end performance model will be developed, capable of mapping errors introduced by system characteristics and measurement uncertainties into the TSCV for realistic range of sea-state parameters. Performance metrics for TSCV (*RMSe, Bias, Resolution, Dynamic Range*) and test scenarios are also outlined in TN2.

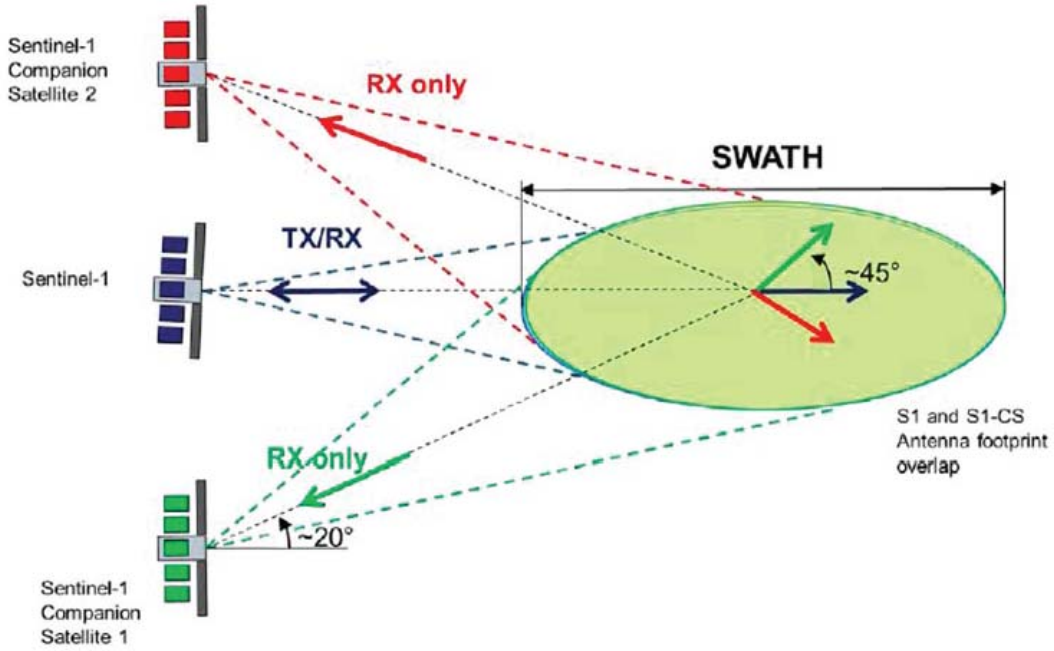


Figure 1 *Schematic illustration of the passive follower concept using a bistatic or stereostatic geometry with Sentinel-1. The figure is taken from [R-2]. When the transmit TX array is electronically steered in elevation or azimuth, the bistatic RX array is steered in 2D to achieve alignment of ground projected principal axis of TX and RX.*

# 2. Review of Scientific Mission Requirements

The total ocean current (TSCV) is the coherent horizontal and vertical movement of surface ocean water (over a specific depth regime) with a given velocity that persist over a geographical area and time period. The horizontal surface current is the dominant part in a stratified ocean with typically velocity in the range 0.1 – 1 m/s. The dynamic processes that create, force and steer the total ocean current vector (TSCV) are complex and include surface wind stress (Ekman current), surface waves (Stokes drift), geostrophic flows, horizontal and vertical thermohaline dynamics, tidal forces all mixed with varying bathymetry and shoreline geometry. Measuring the different contributions to the TSCV is difficult and requires several different types of instruments and measurement principles (ADCP, Drifters, HF radar, satellites). The large-scale geostrophic current is well measured by conventional radar altimeters, and routinely used in models to predict large-scale ocean circulation. However fast moving small scale eddies are not resolved by altimeters, and furthermore the low resolution hampers the applicability of the altimeters in coastal areas. High-resolution SAR have shown capabilities through ATI and DCA measurements to map radial ocean surface velocity field, which can be converted to surface current by removing the Stoke contribution to the measured radial velocity. However, the Stoke contribution is usually the dominant signal in the SAR ATI and DCA unless in areas of strong currents like Agulhas. At present there are no satellites that measure simultaneously the two dominant terms, the Stoke drift and the geostrophic drift. In the recent years, new technologies have been developed like WaveMill[A-2], SKIM [A-3], (and also for land waters, SWOT[A-1]) to better measure simultaneously ocean topography and waves, and the corresponding TSCV. The S1+CS has the potential of further filling the gap, by synergetic combination of NRCS, Image Spectra and DC derived from SAR measurements.

## 2.1. Summary of User Requirements

User requirement for ocean current has recently and extensively been derived in the framework of the ESA GlobCurrent project [A-4]. The requirements are given as geophysical quantities with corresponding accuracy, spatial and temporal sampling, coverage and length of data records. It turns out, not surprisingly, that the majority of the users require higher resolution closer to the coastline (1-2 km) than for the open ocean (10-25km), but with the same measurement accuracy of $\leq$0.2 m/s. This accuracy requires an accuracy of the DCA of around 3Hz at an incidence angle of $23^{o}$ and around 5Hz at $35^{o}$.

In terms of sampling in time, the requirements are hourly products for the coastal areas and daily products for the open ocean areas. For the data latency the requirement is near-real time (i.e. within 3-6 hours).

A comprehensive report on the user requirements for ocean current products can be downloaded from https://globcurrent.nersc.no/system/files/pubdeliver/GlobCurrent_D-020_URD_v4-signed.pdf.

In short the user requirements can be stated as:

- The majority of users want global current data
- The spatial resolution should be 1-2 km in coastal areas and 10-25 km for open ocean
- The time resolution should be between one hour and one day
- The speed uncertainty should be between 5 and 30 cm/s and must be specified per product pixel
- Time series of 10 to 20 years are desired
- The majority of users want access to data in near real-time
- All data products should be compatible with the NetCDF-CF (Climate and Forecast variables) standard

- The product should provide quantification of contributions from Stokes and Ekman drift, and tidal currents

Numerical ocean current model and ocean wave model constitute the ocean component of coupled ocean-atmosphere models. Numerical models have improved significantly the last year much thanks to assimilation of atmosphere and ocean data provided by satellite or by various types of in-situ measurements. Still improvements can be done both on the assimilation scheme and on the quality of the measured ocean and atmosphere data [A-5],[A-6]. For the latter the S1+CS mission can contribute. SAR missions such as Envisat [A-10],[A-11],[A-16] Sentinel-1 [A-12] and TanDEM-X[A-13],[A-14] have already demonstrated the potential of providing ocean surface current measurements both from Doppler Centroid Anomaly (DCA) and Along Track Interferometry (ATI).

The main application and benefit of the SAR ocean current data are expected to be:

- Scientific improvements of numerical large-scale ocean circulation models through advancing ocean data assimilation
- Improved mapping and modelling of the Equatorial current
- Improvement of coastal ocean models through assimilation of ocean current data [A-7]
- Improvement of particle drift models [A-8] tailored to specific application through assimilation of ocean current data
- Application of drift models for prediction of marine debris, oil spill [A-9], search and rescue operations, sea ice drift, iceberg drifts, cod egg drift, aqua culture and harmful alga bloom.

## 2.2. Requirement on Geophysical Calibration of DCA

The ocean Doppler centroid anomaly (DCA) is to first order a sum of the contribution from the underlying surface current and the wind/wave induced drift. The latter contribution is often called the "DCA wave bias". A fundamental requirement for utilizing the DCA for ocean surface current measurement is the ability to precisely predict or measure "DCA wave bias", which is approximated to be proportional to the line-of-sight component of Stoke drift [A-10]. The Stoke drift can be parameterized in terms of wave parameters:

$$(1) \qquad U_S \approx \frac{4\pi^2 a^2}{\lambda T_p} e^{4\pi z/\lambda}$$

where $\alpha, \lambda, T_p$ are the dominant wave amplitude, wavelength and wave period of the wind sea, and $z$ is the depth. Unfortunately, the S1+CS system is in general not suitable to capture waves at wavelengths that mostly contribute to the Stoke drift because of the azimuth cut-off that filters strongly the underlying 2D ocean wind sea wave spectra. At an average wind speed of 7 m/s, azimuth wavelength components shorter than 220 m are not resolved. However, the limitation can be overcome if we are able to extract information on *inverse wave age* ($\gamma = U_{10}/C_p$) from the 2D SAR ocean wave image spectra. In combination with the S1+CS measured *wind vector* a full 2D ocean wave spectra can then be synthesized from analytical wave models [A-15]. ***Research efforts should be put on developing robust methodology/algorithm to extract inverse wave age or wind sea $H_s$ information (or proxy for these) from SAR ocean image spectra.*** To illustrate this, we show in next sections how the geophysical calibration of DCA (i.e. removal of "DCA wave bias") put strong requirements on the accuracy of the local wind and wave field estimates.

### Wind Sea Wave Spectra

The impact of *inverse wave age* on the prediction of the "DCA wave bias" is shown in Figure 2 with the vertical bars corresponding to ±5% change in *inverse wave age*. It can be seen that knowledge of *wave age* or *wind sea* $H_s$ is critical for achieving the required accuracy of ocean surface current (≤0.3 m/s) from DCA measurements. In Figure 3 we predict DCA error as function of error in *inverse wave* age (or *wind sea* $H_s$) around the fully developed sea corresponding to an *inverse wave age* of $\gamma =$

0.84. From Figure 3 we see that at high incidence angles ($\approx 35^o$) a requirement on the *wind sea* $H_s$ accuracy should be $\leq 0.5m$, but for lower incidence angles ($\approx 23^o$) the requirement should be $\leq 0.2m$. At present there exist no algorithms can provide *wind sea* $H_s$ from SAR measurements to the accuracies mentioned above.

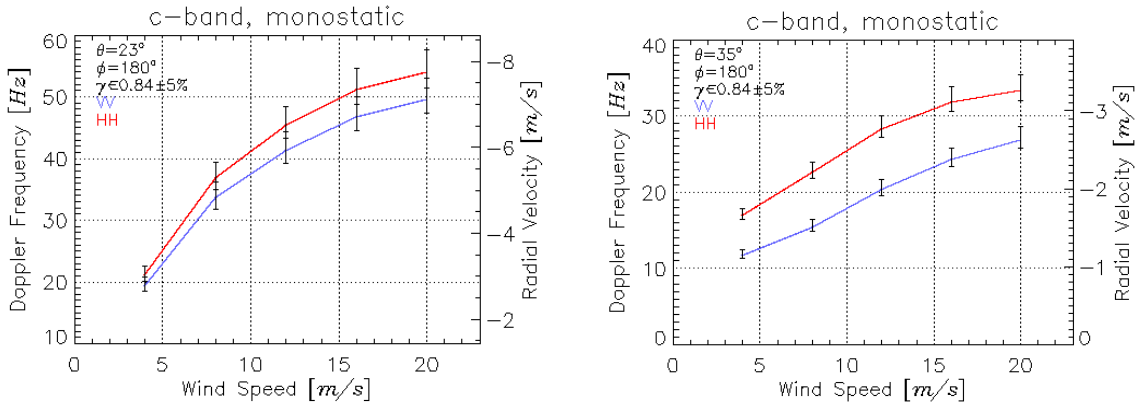


Figure 2 *Simulated "DCA wave bias" (and corresponding radial velocity) as function of wind speed for VV and HH polarizations at incidence angles of 23 deg (left) and 35 deg (right). The vertical bars indicate variations in DCA with ±5% variation in inverse wave age, γ around 0.84. Wind direction is upwind (towards the radar).*

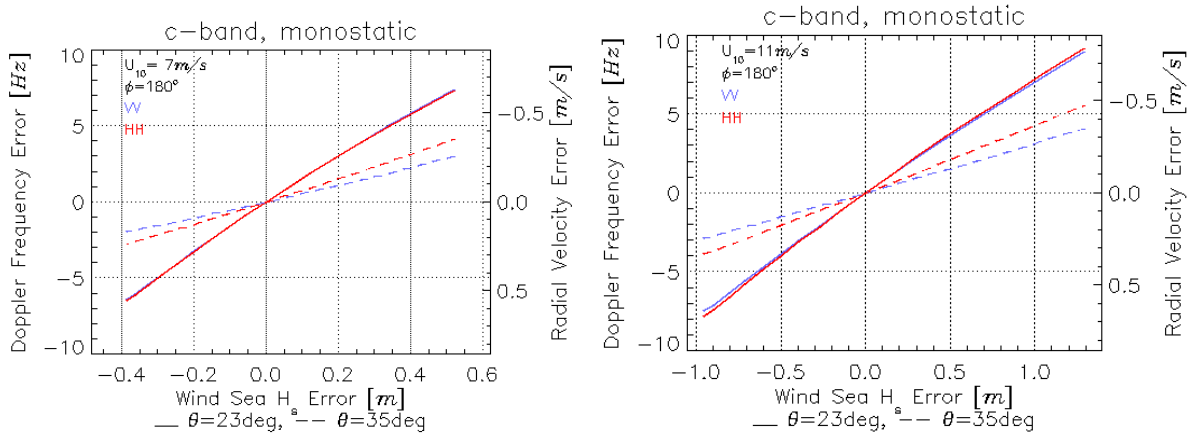


Figure 3 *Simulated DCA (and corresponding radial velocity) errors as function of error in the wind sea* $H_s$ *(around* $H_s$ *for* $\gamma = 0.84$*) for VV and HH polarizations at incidence angles of 23 and 35 degrees. Left plot is for a wind speed of 7m/s and right plot is for 11m/s.*

## Wind Vector

Another critical factor for the geophysical calibration of the measured DCA is the accuracy and resolution of the wind vector used as input to the forward DCA model. In Figure 4 we show simulated errors in DCA at VV and HH polarization as function of incidence angle, given errors in the input wind speed of 1 $m/s$, 1.5 $m/s$ and 2 $m/s$, for two different wind speeds (7 and 11 $m/s$).

In Figure 5 we show errors in DCA as function of incidence angle, given errors in the wind direction of 10 $deg$, 15 $deg$ and 20 $deg$ around the upwind, for two different wind speeds (7 and 11 $m/s$).

The results show that we should aim at predicting the wind speed with an accuracy approaching 1 $m/s$, and the wind direction with an accuracy of 10 $deg$. Again less constrain at high incidence angles.

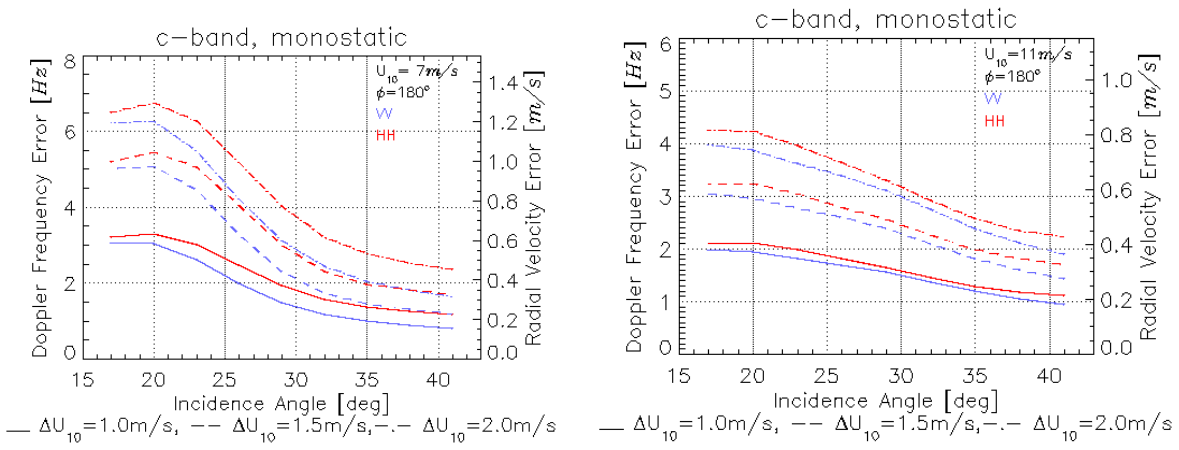


Figure 4 *Simulated VV and HH DCA errors as function of incidence angle with errors of input wind speed of 1m/s (—) 1.5m/s (---) and 2 m/s (-.-.). Left plot is for a wind speed of 7m/s and right plot is for 11m/s. Wind direction is upwind.*

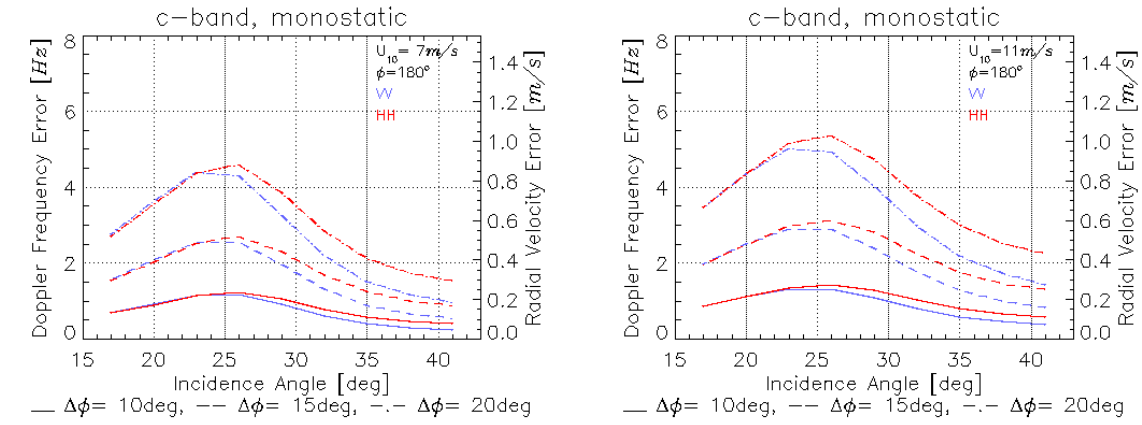


Figure 5 *Simulated VV and HH DCA errors as function of incidence angle with errors of input wind direction of 10deg (___), 20deg (---) and 30 deg (-.-.). Left plot is for a wind speed of 7m/s and right plot is for 11m/s. Mean wind direction is upwind.*

## 2.3. Forward Model Requirements

In this study we have selected forward models based on the closed form approach. This approach fits better to the main objectives of this study, which are the development of TSCV retrieval scheme and an end-to-end (E2E) performance simulator for the S1+CS observing system.

The forward geophysical model functions (GMF) are the engine of the TSCV retrieval methodology and the E2E performance model. The GMFs to be used must be able to provide for both mono- and bistatic geometry and all linear polarizations (hh,vv,vh,hv), the following SAR metrics:

- Normalized radar cross section (NRCS)
- Doppler centroid anomaly (DCA) and Doppler spectra (or Doppler spread)
- 2D Ocean image cross spectra (complex) (CCS)

The input parameters to the closed form GMFs selected for this study are *ocean wind vector*, *inverse wave age* and *surface current vector*. The ocean surface within the GMFs is described statistically with a wave spectra model [A-15]. The GMFs for NRCS and DCA are quite mature, while the CCS must be reconsidered as well as extended to bistatic geometry. This is basically to update the

modulation transfer functions (RAR and SAR MTF) used in mapping the underlying ocean wave spectra to SAR image spectra.

The general parameterisation of the forward GMFs is:

(2) $$GMF = \Gamma\left(U_{10}, \varphi. \underline{v}, \gamma, \theta_i, \theta_s, \phi_s, k_{rad}, pol\right)$$

where

- $U_{10}$ = wind speed $[m/s]$
- $\varphi$ = wind direction relative to range $[deg]$
- $\underline{v}$ = surface current vector relative to range $[m/s]$
- $\gamma$ = inverse wave age $[norm]$
- $\theta_i$ = local radar beam incidence angle $(see\ Fig.6)[deg]$
- $\theta_s$ = local bistatic scattering elevation angle $(see\ Fig.6)[deg]$
- $\phi_s$ = local bistatic scattering azimuth angle $(see\ Fig.6)[deg]$
- $k_{rad}$ = radar wavenumber $[rad/m]$
- $pol$ = radar beam polarization $[hh, vv, hv, vh]$

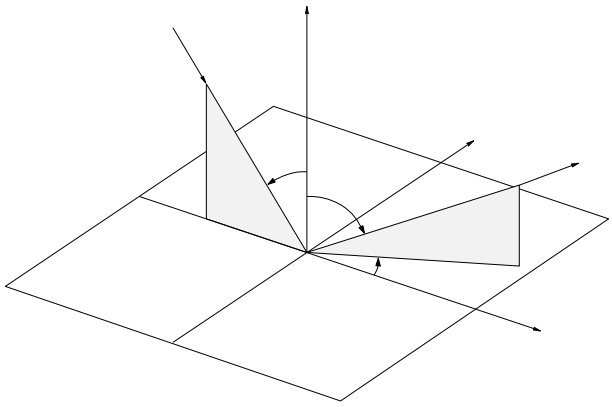

Figure 6 *General 3D bistatic scattering geometry.*

**It should be emphasized at this stage that the forward models outlined in Section 0 and 0 do not include surface current implicitly i.e. current gradients and wave current interactions are not supported (see Romeiser & Thompson, 2000, Hansen et. al. 2010). However, for the Doppler model the direct mean surface current contribution ($2\underline{\mathbf{k}}_{\mathbf{rad}} \cdot \underline{\mathbf{v}}$) is included as part of the retrieval model. This is also the retrieval model concept proposed for the SKIM mission.**

In Section 5 a summary of the features supported by the forward and retrieval models are summarized.

## Scattering and Doppler Models – Python Implementation

The scattering and Doppler model implemented at Ifremer supports various asymptotic methods such as Kirchoff Approximation (KA), Small Slope Approximation (SSA), Geometrical Optics (GO), and Weighted Curvature Approximation (WCA) [A-18]. The available forward bistatic scattering models have been released and published https://www.grss-ieee.org/publication-category/rscl/.

Python notebooks, containing the forward model implementation, have been shared with the team and source code is available on request from Ifremer. Standard configurations have been implemented and basic input parameters listed below can be changed to investigate sensibilities and simulate S1+CS system parameters.

Validation has been done against other models including semi-empirical models for the mono-static case (see Figure 7).

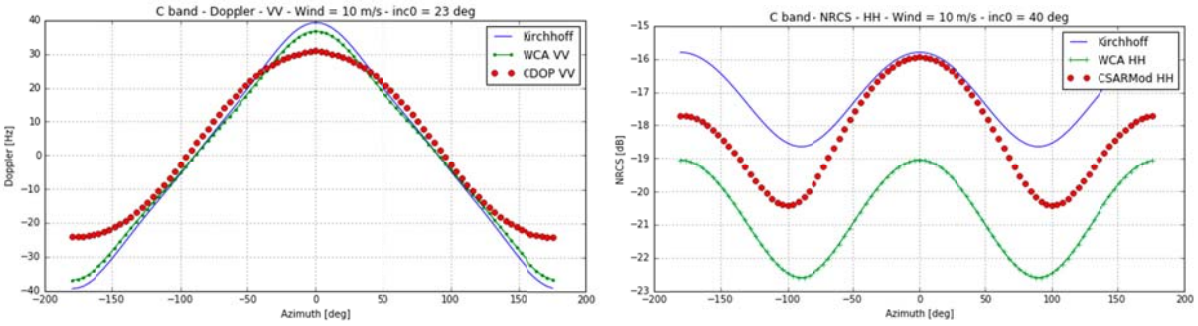


Figure 7 *Left: DCA as function of azimuth angle. Right: NRCS as function of azimuth angle. The red dots are semi-empirical models for DCA (CDOP) and NRCS (CSARMod), included for comparison.*

## Input/Output Data:

Input system parameters:

- Incidence and azimuth angle – ongoing wave [deg]
- Bistatic elevation and azimuth scattering angle – outgoing wave [deg]
- Radar frequency/wavelength [rad/m]
- Radar polarization [vv, hh]

Input geophysical parameters:

- Wind speed [m/s]
- Wind direction [degRa]
- Different wave spectra models
- Electric permittivity

Output parameters:

- NRCS [dB]
- Geophysical Doppler Shift [Hz]
- Product format: TBD

## Required Updates:

As part of Task 2, the forward model implementation will be extended with the following elements:

- Implementation of upwind/downwind asymmetries for
  - NRCS

- Doppler shifts

- Implementation of Reduced Curvature Approximation (RCA)
- Eulerian/Lagrangian harmonization for Doppler approach
- Cross-polarization

## Scattering and Doppler Models – IDL Implementation

The software is written in IDL and stored and maintained in Norut gitLab repository (gitlab.itek.norut.no). The software can be made available on request from Norut. Currently, it only supports mono-static scattering geometry.

Scattering Model:

The backscattering model implemented at Norut is based on the theoretical works documented in the papers [A-19],[A-20],[A-24]. The first paper [A-19] describes the analytic scattering model (General Curvature Model - GCM), which is based on evaluating the scattering integral by a curvature expansion of the fields at an elevated non-perfect conducting regular surface. The model supports vv, hh and cross-polarisation as well as different radar frequencies and incidence angles. A Lagrangian surface model is used providing "Stokes-like" waves with sharper crest and wider trough. However, this version did not include effects of breaking waves nor the effect of wave skewness. These effects were included into the extension of the backscattering model as described in paper [A-20],[A-21], respectively. The effect of breaking waves (non-Bragg) is included using the model of [A-25] providing the total NRCS on the form:

$$\sigma_o^{\alpha\alpha} = \sigma_{gcm}^{\alpha\alpha} \cdot (1-q) + \sigma_{wb} q \qquad \alpha\alpha \in \{hh, vv, hv\} \tag{3}$$

where $\sigma_{gcm}^{\alpha\alpha}$ is the NRCS from the GCM model, which inherently includes both specular and Bragg scattering terms from regular surface. $\sigma_{wb}$ is the non-Bragg term from breaking waves, and $q$ is the fraction of area on the surface that breaks computed from the wind sea spectral model. The final extension of the monostatic GCM model was to include skewness in the wave field (see Figure 8). This extension provides upwind/ downwind asymmetry in NRCS even for low winds where no wave breaking occurs.

The software can be run with and without skewness and with two different upwind/downwind skewness coefficients, either Breon or Cox [A-26]. These skewness coefficients are both driven by the wind speed.

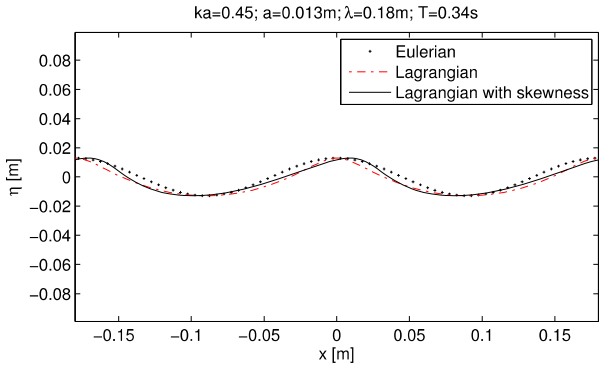


Figure 8 *1-D deep-water small surface wave profile using a Eulerian, a Lagrangian, and a Lagrangian with skewness approaches. Wave parameters such as wave steepness, wave amplitude, wavelength, and period are shown above the plot (from [A-20])*

The model implementation has been validated extensively against Cmod5.n, and quantitative results can be found in [A-20]. Example is shown in Figure 9. A good agreement between the upwind/downwind asymmetry of the extended GCM and Cmod5.n is achieved for moderate winds (≈5–10 m/s) and moderate incidence angles (≈32◦–40◦). For low incidence angles (<26◦), the GCM tends to overestimate the upwind/downwind asymmetry compared with CMOD5.n.

The input/output parameters are listed below.

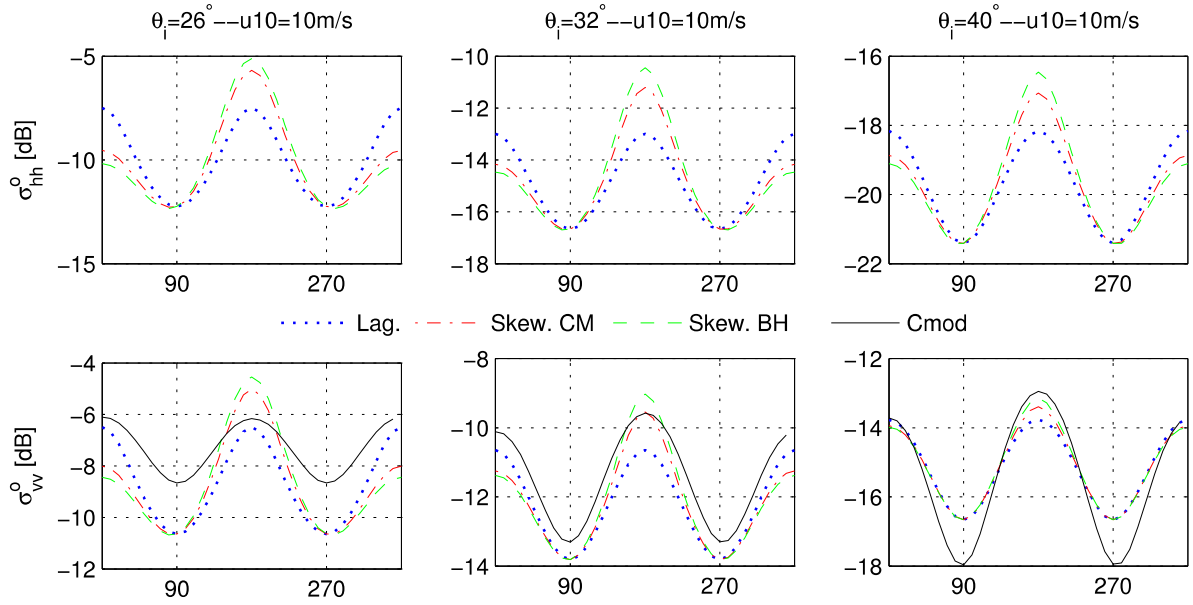


Figure 9 *Comparison of NRCS from backscatter model with and without skewness parameters as function of wind direction relative to range (0 is downwind) for three incidence angle and wind speed of 10 m/s. Upper plots are HH polarization and lower are VV polarization. For VV polarization the NRCS from Cmod5.n is overplotted (from [A-20]). Here Lag means only Lagrangian, CM means Cox&Munk skewness parameter, and BH means Breon skewness parameter.*

## Doppler Model

The Doppler model implemented at Norut is based on the theoretical work first documented in paper [A-23] based on the first version of the GCM backscattering model. Later the Doppler model was extended [A-22], to include the latest backscattering model as described in Section 0 including both wave skewness and breaking waves. The latter paper also contains comparison against the semi-empirical Doppler model – CDOP (see Figure 10). The formalism of the Norut DCA model from regular surface is a bit different from previous models in the sense that it is directly derived from spectral moments (first and zero) of the spectra of the theoretical expression for the complex SLC image. The formalism is then similar to the way we estimate DC from an SLC image i.e. as a frequency shift of the azimuth spectra of the SLC image. The contribution to the DCA from breaking waves is added to the regular wave DCA using the same approach as for the NRCS. Explicitly we write for the total DCA:

$$f_{dc}^{\alpha\alpha} = P_{gcm}^{\alpha\alpha} f_{gcm}^{\alpha\alpha} \cdot (1-q) + P_{wb}^{\alpha\alpha} f_{wb}^{\alpha\alpha} q \qquad \alpha\alpha \in \{hh, vv, hv\} \tag{4}$$

where the coefficients $P$ is the backscatter ratio of the respective scattering model NRCS and the total NRCS, and again $q$ is the fraction of breaking waves.

The software is implemented in IDL, and computes both the NRCS and DCA in the same run. The data are stored in a netCDF file. The input/output parameters are listed below.

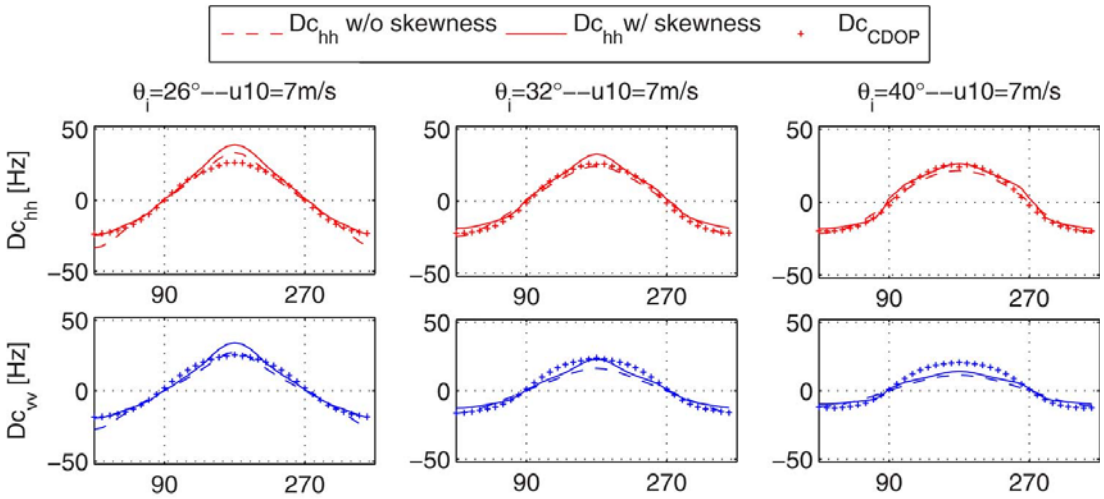


Figure 10 *Comparison of GCM DCA model output with and without skewness as function of wind direction (0 is downwind) for three incidence angles and wind speed of 5 m/s. The full lines are DCA from CDOP (from [A-22]).*

## Input/Output Data:

Input system parameters:

- Incidence Angle [deg] ; supports array
- Radar wavenumber [rad/m]
- Radar polarization [vv, hh,vh,hv] ; supports array of string

Input geophysical parameters (min, max and number of values):

- Wind speed [m/s]
- Wind direction [degRa]
- Inverse wave age [norm.]

Output data:

- NRCS [dB]
- DCA [Hz],
- DCA spread [Hz]
- Format – netCDF

## Required Updates:

Extending the code to support bistatic configuration of S1+CS.

## Ocean-to-SAR Spectral Model – IDL Implementation

The spectral forward model implementation is based on an approximate version of the closed from ocean-to-SAR cross-spectral transform [A-27]. The actual analytical form implemented is given as:

$$P(\underline{k},t) = \int e^{k_y^2\left(\rho_{\xi\xi}(\underline{x},t)-\rho_{\xi\xi}(0,0)\right)}\{1+a(k_y,\underline{x},t)\}e^{-i\underline{k}\cdot\underline{x}}d\underline{x} - \delta(\underline{k}) \quad (5)$$

where $a(k_y,\underline{x},t) = \rho_{\sigma\sigma}(\underline{x},t) + ik_y\left(\rho_{\sigma\xi}(\underline{x},t) - \rho_{\xi\sigma}(\underline{x},t)\right)$. Here, $P$ is the SAR image cross spectra as function of wave-vector $\underline{k} = (k_x, k_y)$ (range, azimuth) and $t$ is the look separation time. $\rho_{\xi\xi}$, $\rho_{\xi\sigma}, \rho_{\sigma\xi}$ and $\rho_{\sigma\sigma}$ are cross covariance functions between the azimuth shift field $\xi = \frac{R}{V}U_r$ caused by the range component of the orbital velocity of the waves, $U_r$, and the modulation field $\sigma$ of the radar backscatter cross section. These fields are generally written in terms of MTFs $T_l, T_m$ and the underlying ocean wave spectra, $S$ as:

$$\rho_{lm}(\underline{x},t) = \frac{1}{(2\pi)^2}\int\left\{\frac{1}{2}T_l(\underline{k})T_m^*(\underline{k})e^{-i\omega_{|k|}\cdot t}S(\underline{k}) + \frac{1}{2}T_l(-\underline{k})T_m^*(-\underline{k})e^{i\omega_{|k|}\cdot t}S(-\underline{k})\right\}d\underline{k} \quad (6)$$

where $l \in \{\xi,\sigma\}, m \in \{\xi,\sigma\}$ and $\omega_{|\underline{k}|}$ is ocean wave dispersion relation. The underlying wave spectra, $S$ is computed from the spectral model of [A-15]. The modulation transfer function of $\sigma$ is computed from a backscatter model.

The transform can be shown to be a sum of non-linear (mainly wind driven) part and a quasi-linear (mainly swell driven) part:

$$P(\underline{k},t) = P_{nlin}(\underline{k},t) + P_{qlin}(\underline{k},t) \quad (7)$$

where the quasi-linear part can be written as $P_{qlin}(\underline{k},t) = e^{-k_y^2\rho_{\xi\xi}(0,0)}\int\{k_y^2\rho_{\xi\xi}(\underline{x},t) + a(k_y,\underline{x},t)\}e^{-i\underline{k}\cdot\underline{x}}d\underline{x}$. Here the exponential cut-off factor is given as $\rho_{\xi\xi}(0,0) = \frac{1}{2\pi}\int|T_\xi(\underline{k})|^2 S(\underline{k})d\underline{k}$ where $T_\xi$ is the azimuth shift (velocity bunching) MTF given as $T_\xi(\underline{k}) = \frac{R}{V}\omega_{|k|}\left\{\frac{k_x}{|\underline{k}|}\sin\theta + i\cos\theta\right\}$. And $\frac{R}{V}$ is the range to velocity ratio and $\theta$ is the incidence angle. The non-linear part (Eq.(7) can be written as:

$$\begin{aligned} P_{nlin}(\underline{k},t) = e^{-k_y^2\rho_{\xi\xi}(0,0)}\Big\{&\int\left[e^{-k_y^2\rho_{\xi\xi}(\underline{x},t)} - 1 - k_y^2\rho_{\xi\xi}(\underline{x},t)\right]e^{-i\underline{k}\cdot\underline{x}}d\underline{x} \\ &+ \int\left[e^{-k_y^2\rho_{\xi\xi}(\underline{x},t)} - 1\right]a(k_y,\underline{x},t)e^{-i\underline{k}\cdot\underline{x}}d\underline{x}\Big\} \end{aligned} \quad (8)$$

The full spectra (Eq.(7)) and the quasi-linear spectra ($P_{qlin}$) are both outputs from the simulator. An example is shown in Figure 11 and Figure 12. Note that the non-linear part vanishes at range axis, $k_y = 0$. The input/output parameters are listed below.

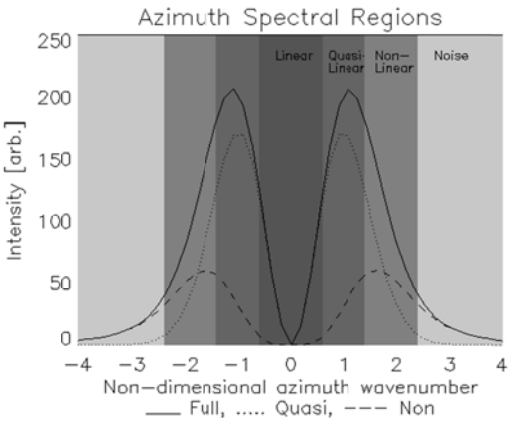


Figure 11 *Simulated azimuth spectral profiles for the quasi-linear, non-linear, and full SAR spectra. The shaded areas illustrate the different imaging areas in azimuth wavenumber domain. The non-dimensional azimuth wavenumber is* $\kappa \equiv k_y \sqrt{\rho_{\xi\xi}(\underline{0}, 0)}$.

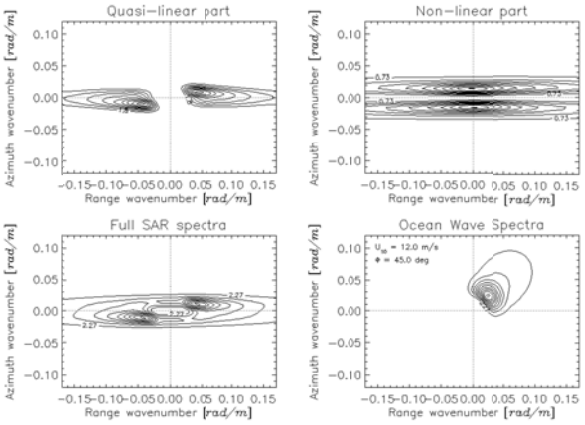


Figure 12 *Simulated cross-spectra wind speed of 12 m/s and wind direction of 45 degrees relative to range axis. ul) quasi-linear part, ur) non-linear part, ll) full SAR spectra, lr) corresponding input ocean wave spectra.*

## Input/Output Data:

Input system parameters:

- Swath (Sentinel-1) [is1,is2,is3,is4,is5]
- Radar wavenumber [rad/m]
- Radar velocity [m/s]
- Azimuth resolution [m]
- Ground range resolution [m]
- Satellite height [m]
- Radar polarization [vv, hh, vh, hv]

Input geophysical parameters (min, max and number of values):

- Wind speed [m/s]
- Wind direction [degRa]
- Inverse wave age [norm.]
- Look separation time [sec]

Output spectral data:

- SAR ocean image cross-spectra (real and imaginary part)
- Quasi-linear part of SAR ocean image cross-spectra (real and imaginary part)
- Format (TBD)

Output meta data:

- List of meta data describing the content (type,size,…) of spectral data
- List of computed $H_s$, NRCS and RAR MTF amplitude versus input wind field
- Output format: info file (text), data file (binary)

## Required Updates:

The current version of the spectral forward simulator does not support bistatic geometry or the existence of surface current. In the S1+CS inversion scheme the phase of the cross spectra in the linear region is important since it is used for consistency check of the Doppler retrieved surface current. Below we describe a possible extension of the spectral simulator to meet these needs.

### Wave Spectra in Uniform Current Field:

In linear wave theory the dispersion relation will be modified as:

$$\omega(k) = \pm\omega_{|k|} + \underline{v} \cdot \underline{k} \quad (9)$$

where $\omega_{|k|} = \sqrt{gk}$ is the dispersion relation for deep water waves, and $\underline{v} \cdot \underline{k} = vk\cos(\phi - \beta)$ where $\phi - \beta$ is the angle between wave direction and surface current direction.

Wave spectra (given as a product between heave and the normalized directional spectra) in a steady current as seen by an observer can be written as:

$$S(\omega) \cdot D(\omega, \phi) = \frac{C_g(k)}{|C_g(k) + v\cos(\phi - \beta)|} S_o\left(\omega_{|k|}\right) \cdot D_o\left(\omega_{|k|}, \phi\right) \quad (10)$$

where $C_g$ is the group velocity, and indexes 0 refers to spectra in a system moving along the direction of the current. Here $k$ on the right hand side of Eq.(10) is the solution of the dispersion relation given in Eq.(9). The forward simulator can be updated by adding a module that modifies the computed wave spectra and dispersion relation according to Eq.(9) Eq.(10). Example of simulated phase and spectral profiles in a current regime are shown in Figure 13. The integrated phase difference over the spectral peak between no current and with current will be used in the inversion scheme to check consistency of the first iteration on the surface current.

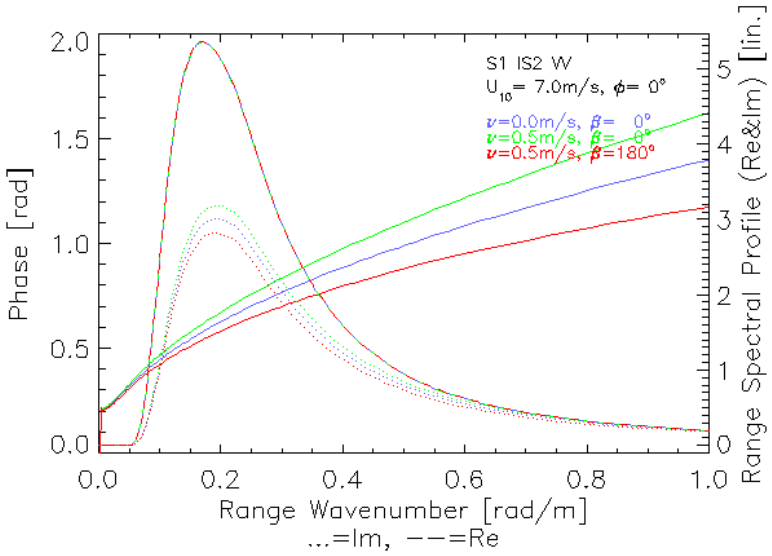


Figure 13 *Phase (__) and spectral range profiles (---=real part, ….= imaginary part) of simulated SAR cross spectra with different current directions (downwave ( $\beta = 0^o$), and upwave ($\beta = 180^o$), and speeds ($\upsilon = 0\ m/s$ and $\upsilon = 0.5\ m/s$). Wind direction is downwind ($\phi = 0^o$).*

Bistatic Geometry:

The whole ocean-to-SAR spectral transform must be reconsidered for bistatic geometry. The bistatic geometry will modify the MTF used in Eq.(6). In the mono-static version the RAR MTF is computed from a backscatter model.

Phase Spectra and Dispersion Relation:

The proposed surface current retrieval scheme (Section 0) for the high-bandwidth modes of S1 intends to use the SAR spectral phase information to check for consistency. However, the existing version of the forward model does not properly reflect the phase or in general the range spectral profile observed in S1 data. While the phase of the simulated spectra (see Figure 13) has a linear behaviour along range axis (only classic dispersion relation phase), the observed phase or dispersion shows a different behaviour as shown in Figure 14. In general the dispersion relation observed in the S1 WV data is lower than expected from linear theory. This indicates that there is non-linearity in the imaging along the range axis and/or that the effective look separation time is shorter than expected.

Furthermore, the phase signal from a single measurement in the S1 WV or SM modes is rather noisy due to the short look separation time ($\tau \approx 0.36sec$). For the S1 IW mode, both high range resolution and large look separation time ($\tau \approx 2.5$sec) can be achieved in the burst overlap areas, causing a much stronger phase signal as shown in Figure 15. Such data are also in much better agreement with the linear dispersion relation for the peak of the spectra.

Another critical factor is also whether or not the surface current signal is strong enough to be detectable in the spectral phase of a single S1 measurement. As can be seen from Figure 13, the simulated impact of a surface current is rather small on the phase.

***Research is needed to better describe and understand the forward cross-spectral model with and without the presence of a surface current.***

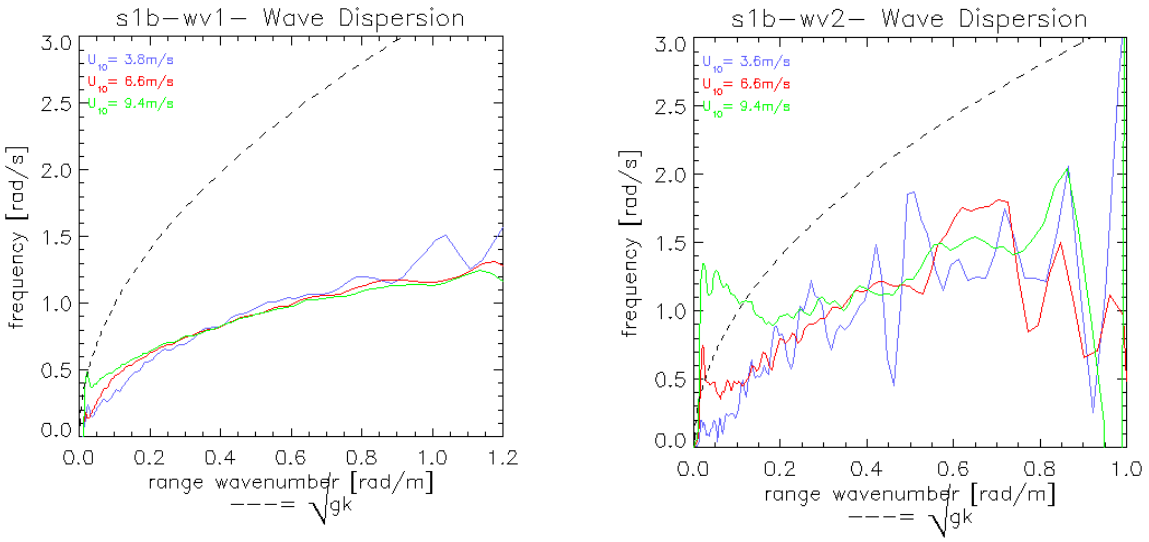


Figure 14 *Mean S1b WV wave dispersion for different wind speeds at downwind. Dotted line is the linear dispersion relation. Left : WV1, Right: WV2*

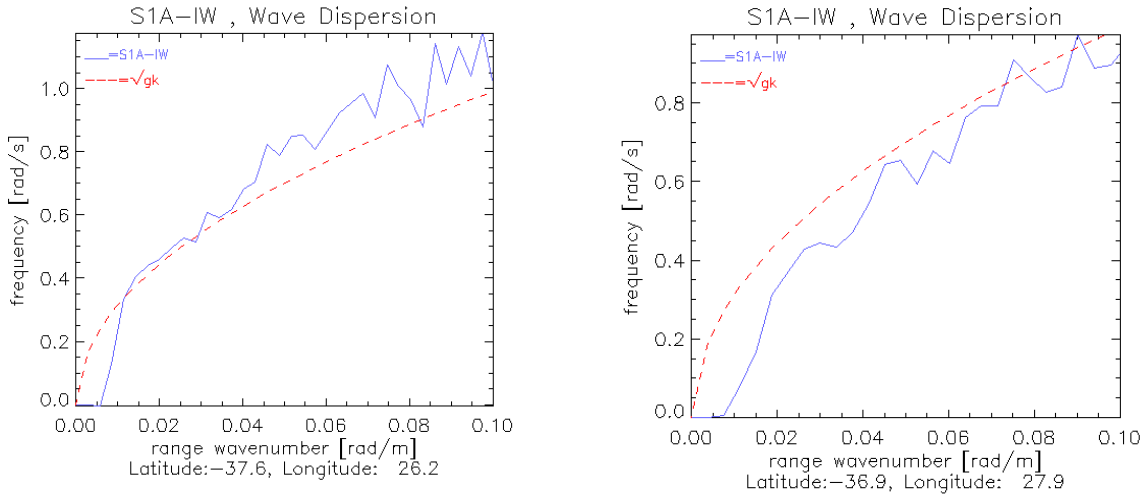


Figure 15 *Single measurement wave dispersion extracted from burst overlap area of S1a IW acquired over Agulhas. ymdh: 20160115T170826. Left: IW1, Right: IW3*

### Adaption to S1+CS TSCV retrieval

The forward models describe above requires adaption to the S1+CS TSCV retrieval approach outlined in Section 0. The forward models must be linked such as to produce all the necessary mapping between input and output geophysical parameters needed for the inverse GMF´s to be used in the retrieval scheme. To avoid computation time and to provide a clean interface, a look-up table (in netCDF format) can be used to provide the inputs to the retrieval scheme. Furthermore, the complex 2D image cross spectra from the forward model needs to be converted to the specific spectral metrix used in the inversion scheme. Efforts should be put on finding cross-spectral parameters as proxies for wind/wave/current parameters.

## 2.4. Retrieval Model Requirements

### Retrieval model concept

The retrieval model is based on the forward GMFs and the S1+CS system error models. A surface current retrieval model needs ideally to be based on a coupled wind/wave/current retrieval approach in order to accommodate for the coupling of surface roughness and kinematics manifested in SAR measurements. This requires collocated (in time and space) knowledge of sea-state and wind field.

The usual OSC retrieval is the direct approach, which neglects the sea state information and performs a prediction of the *DCA wave bias* using CDOP with only external model wind field as input. The residual DCA between the measured DCA and the predicted *DCA wave bias* is then converted to LOS surface current.

$$(11) \quad v_r = -\frac{\pi\left(f_{dc}^{obs} - f_{dc}^{cdop}\right)}{k_{rad}}$$

The weak points of this approach are: - neglecting of sea state in the CDOP function as quantified in Figure 3, - the use of model wind field, which may introduce errors for instance due to coarser time/space resolution. Impact on DCA due to errors in wind field is quantified in Figure 4 and Figure 5. The accuracy achieved with this method as compared to drifter is at best around 0.4 m/s [A-12], [A-16], [A-17]. It is likely to believe that most of the uncertainty comes from errors in the prediction of the "DCA wave bias". Over sea ice, where the "DCA wave bias" is negligible, much better agreement ($< 0.1 m/s$) is achieved between sea ice drift derived from DCA and from feature cross-correlation [A-28].

The proposed S1+CS OSC retrieval scheme builds on experience from monostatic SAR systems and is extended to bistatic SAR systems by adapting the observation geometry to the contributing scatterers bistatic facets, but also to solve consistently for both wind vector and surface current without using model wind field. The inputs considered for this TSCV retrieval are, for each of the three receiving antennas (one active and two passive), the NRCS, the DCA and the Image Cross Spectra. The S1+CS TSCV retrieval scheme will also incorporate S1+CS system and measurement errors. The use of metrixes extracted from the Image Cross Spectra can help us avoid the use of model wind field, at least for the high range bandwidth data (i.e. WV, SM and IW modes) of S1+CS. For EW mode, a degraded approach is proposed where we rely on the use of ancillary model wind field. The retrieval approach can be divided into the following four steps:

The first step is to estimate $10m$ wind vector $\underline{U}_{10}$ and inverse wave age, $\gamma$ from NRCS ($\sigma$) and Image Cross Spectra (sp) by minimization the cost fuction $J1$:

$$(12) \quad J1\left(\underline{U}_{10}, \gamma\right) = \sum_{j\in\{s1,cs1,cs2\}} \frac{\left(\sigma_{o-mod}^{(j)}\left(\underline{U}_{10}\right) - \sigma_{o-obs}^{(j)}\right)^2}{Var\left(\sigma_{o-obs}^{(j)}\right)} + \frac{\left(sp_{mod}^{(j)}\left(\underline{U}_{10}, \gamma\right) - sp_{obs}^{(j)}\right)^2}{Var\left(sp_{obs}^{(j)}\right)}$$

where the summation $j$ is over the S1 and the CS measurements, and the subscript *mod* means the predicted GMF values and *obs* means the corresponding value estimated from the S1+CS data. The

spectral parameters, $sp$ will be extracted from separated region of the cross-spectra such as to track both the wind driven and the wave age impacted spectral areas. The *Var* means the variance, which depends on the S1+CS system and measurements errors. This cost-function approach is similar to the one developed for the multi-antenna "WaveMill" (+/- 45 degree) system.

The second step provides a first iteration of the surface current vector, $\underline{v}$. We start with estimating the expected *DCA wave bias* ($f_{dc-wave}$) using the forward DCA model with inputs $\underline{U}_{10}$ and $\gamma$. Then we take the difference between observed DCA and the *DCA wave bias* and compute the first iteration on the radial surface current components for each of the three antennas:

$$(13) \quad v_r^{(j)} = -\frac{\pi\left(f_{dc-obs}^{(j)} - f_{dc-wave}^{(j)}\big|_{\underline{U}_{10},\gamma}\right)}{k_{rad}} \qquad j \in \{s1, cs1, cs2\}$$

The third step performs a refinement of wind vector using the first guess surface current, followed by a final iteration on the surface current. First a consistency check is performed by comparing the observed phase speed from the image cross spectra (in the linear region) with the simulated phase speed (from the forward model of Section 0) including the first guess surface current ($v_{ph} = \pm\sqrt{g/k} + v\cos\beta$), where $\beta$ is the angle between surface current and wave direction. If consistency is achieved, a refinement of the wind vector is performed by minimization the cost function $J2$, where we now compensate for the existence of the surface current vector, $\underline{v}$. If not, no TSCV estimate is provided.

$$(14) \quad J2\left(\underline{U}_{10}\right) = \sum_{j\in\{s1,cs1,cs2\}} \frac{\left(f_{dc-wave}^{(j)}(\underline{U}_{10},\gamma) - \Delta f_{dc-obs}^{(j)}\right)^2}{Var\left(\Delta f_{dc-obs}^{(j)}\right)} + \frac{\left(\sigma_{o-mod}^{(j)}(\underline{U}_{10})\big|_{\underline{v}} - \sigma_{o-obs}^{(j)}\right)^2}{Var\left(\sigma_{o-obs}^{(j)}\right)} + \frac{\left(sp_{mod}^{(j)}(\underline{U}_{10},\gamma)\big|_{\underline{v}} - sp_{obs}^{(j)}\right)^2}{Var\left(sp_{obs}^{(j)}\right)}$$

where the first term is the difference between *DCA wave bias* model and the residual $DCA$ estimated itself from the difference between observed Doppler and the predicted surface current, $\underline{v}$ induced Doppler $\left(\Delta f_{dc-obs}{}^{(j)} = f_{dc-obs}{}^{(j)} - \frac{1}{\pi}\left|\underline{k}_{rad}\right|v_r^{(j)}\right)$. The second term is the difference between observed NRCS and modeled NRCS based on using both $\underline{U}_{10}$ and $\underline{v}$. The third term is the difference between observed cross-spectral parameter and modeled cross-spectral parameter, where the latter includes a modification due to surface current, $\underline{v}$.

The final step is the second iteration on the surface current components using again Eq. (13), but now with the refined wind vector, $\underline{U}_{10}$ as input to the *DCA wave bias* model. The final surface current vector in the azimuth, ground range plane $\left(\underline{\hat{x}}, \underline{\hat{y}}\right)$ (see Figure 16) can then established by combining the radial components, $v_r^{(j)}$ from mono-static and bi-static geometries as follows:

$$(15) \quad \begin{aligned} \underline{U} &= \frac{v_r^{s1}}{\sin\theta_{s1}}\left(\underline{\hat{x}} + \tan\phi\cdot\underline{\hat{y}}\right) \\ \phi &= \tan^{-1}\left(\frac{v_r^{cs1}/\sin\theta_{cs1} - v_r^{cs2}/\sin\theta_{cs2}}{\left(2v_r^{s1}/\sin\theta_{s1}\right)\sin\psi_{cs}}\right) \end{aligned}$$

where $\phi$ is the surface current direction relative to S1 radar line of sight and $\psi_{cs} = \psi_{cs1} = -\psi_{cs2}$ is the angle between the S1 plane of incidence and the bisector planes of CS1 and CS2.

And $\theta_{s1}, \theta_{cs1},, \theta_{cs2}$ are the incidence angles of S1 (i.e. in the plane of incidence) and of the CS1 and CS2 (i.e. in the bisector planes), respectively. The relation between the S1+CS radial surface current components and the total surface current vector is illustrated in Figure 16.

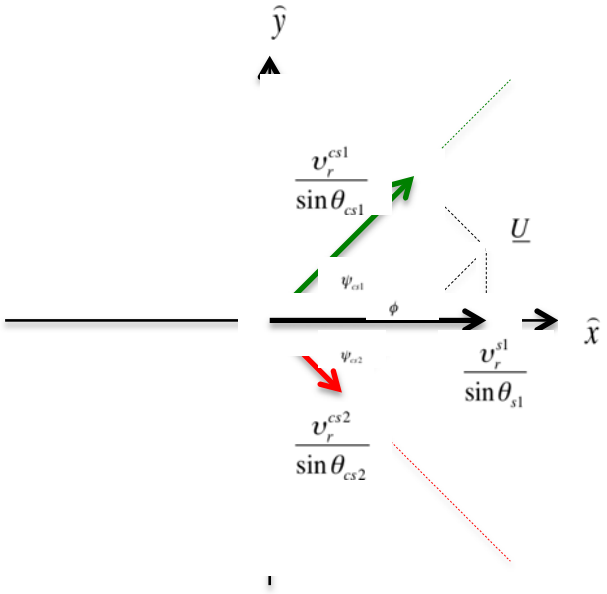


Figure 16 *Relation between the radial surface current vector components of S1+CS and the total surface current vector U at an angle of $\phi$ with respect to S1 ground range.*

A graphical illustration of the retrieval steps is given in Figure 17 applicable for the WV, SM and IW mode. The retrieval steps for the degraded approach applicable for the EW mode are shown in Figure 18.

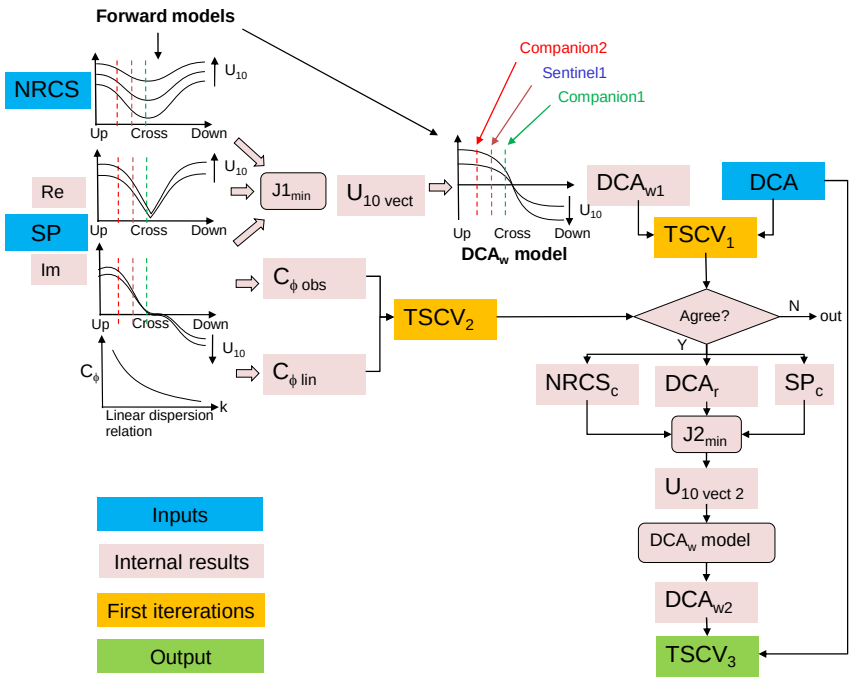


Figure 17 *High-level retrieval scheme for the TSCV from S1+CS observations.*

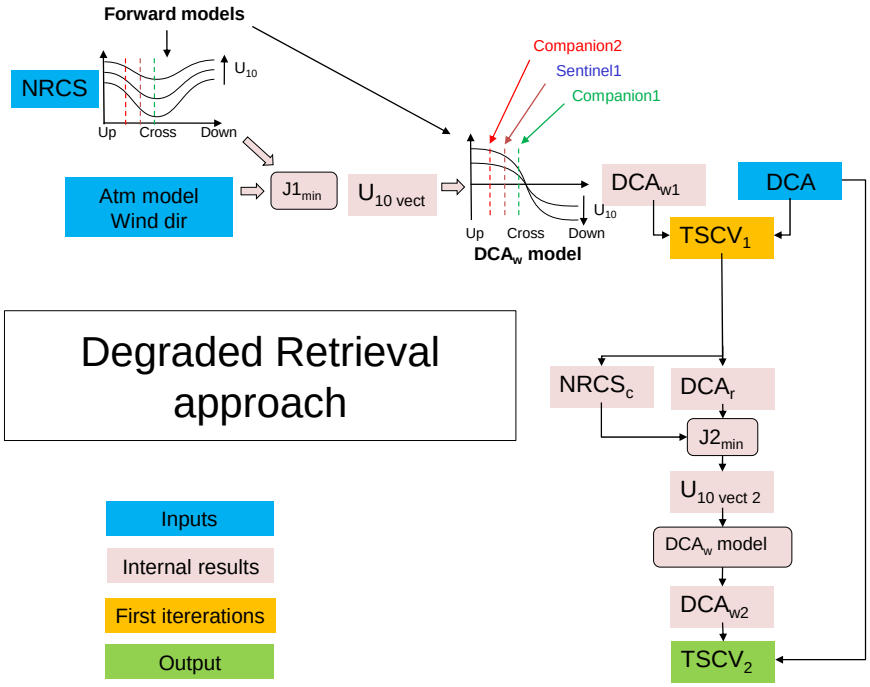


Figure 18 *High-level degraded retrieval scheme for the TSCV from S1+CS observations.*

## Input/Output Data:

Input system parameters:

- Local radar incidence angle
- Local radar bistatic scattering elevation angle
- Local radar bistatic scattering azimuth angle
- Radar wavenumber
- Radar polarization

Input data

- Triplets of observed NRCS, DCA and Cross-Spectra
- Triplets of observation uncertainty of NRCS, DCA and Cross-Spectra
- Look-up tables (netCDF) of pre-computed triplets of NRCS, DCA and Cross-Spectra as function of wind and current fields. These are pre-computed using the forward models.

Output data:

- Wind field
- Current field

## Required Updates:

Include the retrieval of inverse wave age or equivalently the wind sea waveheight as part of the wind retrieval.

# 3. Doppler Calibration

It is important to notice that the measured Doppler centroid frequency is in general a sum of contribution from geometry (satellite attitude and antenna) and geophysics (surface motion). The geometric terms must be predicted and removed to the same accuracy as required for the final DCA. Experiences with Sentinel-1a and b show that the requirement of an absolute calibration of the estimated DC to better than 5Hz put strong requirement on the attitude prediction along the orbit as well as on the prediction of the antenna electronic miss pointing DC bias. Although this is put in place at best practice, experiences show that a data driven refinement of the DC calibration is needed. The following task should be put in place to achieve the goal of fully calibrated DC from S1+CS:

- Access to precise attitude data. Software to compute the DC from attitude and vice versa for S1 and the followers
- Access to antenna model. Software to compute electronic miss pointing DC bias from S1+CS antenna models.
- Generation of EM DC bias correction profiles. Assessment of antenna time stability on cycle basis by routine monitoring of mismatch between data estimated and model predicted EM miss pointing DC bias. Provision of mean electronic miss pointing DC bias correction profile on cycle basis. For this the TOPS mode land acquisitions should be used.
- Generation of refined attitude file. This can be done by a data driven approach that minimizes (along orbit segments) the difference between observed DC and the computed "DCA wave bias" with respect to a simple parametric model for the residual attitude+EM DC. The total updated attitude+EM DC is then used to generate a refined attitude file. For this the S1 WV mode must be used.
- DC calibration work flow: An operational work flow that generates the above mentioned DC correction data and refined attitude files, and performs an absolute calibration of the measured DC for all S1 modes. The precise DC calibration should ideally be an integrated part of the Level 2 processor.

# 4. References

T. Börner, P. López Dekker, G. Krieger, M. Bachman, A. Moreira, H. Müller, "Passive Interferometric Ocean Currents Observation Synthetic Aperture Radar (PICOSAR)", 9th IAA Symposium on Small Satellites for Earth Observation

R. Bamler, "Doppler frequency estimation and the Cramer-Rao bound", IEEE Transactions on Geoscience and Remote Sensing, Vol. 29, Issue 3, May 1991

K.F. Dagestad, J. A. Johannessen, H. Johnsen, G. Engen, "Ocean currents performance models for bi-static Sentinel-1 companion", NERSC Technical Report No. 318, 2011

A. A. Mouche, F. Collard, B. Chapron, K. F. Dagestad, G. Guittion, J. A. Johannessen, V. Kerbaol, M. W. Hansen On the use of Doppler shift for sea surface wind retrieval from SAR, IEEE Trans. Geoscience and Remote.

Nouguier Frederic, Guerin Charles-Antoine, Soriano Gabriel (2011). Analytical Techniques for the Doppler Signature of Sea Surfaces in the Microwave Regime-I: Linear Surfaces . IEEE Transactions On Geoscience And Remote Sensing , 49(12), 4856-4864.

Nouguier Frederic, Guerin Charles-Antoine, Soriano Gabriel (2011). Analytical Techniques for the Doppler Signature of Sea Surfaces in the Microwave Regime-II: Nonlinear Surfaces . IEEE Transactions On Geoscience And Remote Sensing , 49(12), 4920-4927

Guerin Charles-Antoine, Soriano Gabriel, Chapron Bertrand (2010). The weighted curvature approximation in scattering from sea surfaces . Waves In Random And Complex Media , 20(3), 364-384

Mouche Alexis, Chapron Bertrand, Reul Nicolas, Collard F (2008). Predicted Doppler shifts induced by ocean surface wave displacements using asymptotic electromagnetic wave scattering theories . Waves in Random and Complex Media , 18(1), 185-196

Mouche Alexis, Chapron Bertrand, Reul Nicolas (2007). A simplified asymptotic theory for ocean surface electromagnetic wave scattering . Waves in Random and Complex Media , 17(3), 321-341

Ardhuin Fabrice, Gille Sarah T., Menemenlis Dimitris, Rocha Cesar B., Rascle Nicolas, Chapron Bertrand, Gula Jonathan, Molemaker Jeroen Small-scale open-ocean currents have large effects on wind-wave heights, Journal of Geophysical Research: Oceans IN PRESS . http://doi.org/10.1002/2016JC012413

Kudryavtsev Vladimir, Yurovskaya Maria, Chapron Bertrand, Collard Fabrice, Donlon Craig (2017). Sun glitter imagery of surface waves. Part 2: Waves transformation on ocean currents, Journal Of Geophysical Research-oceans , 122(2), 1384-1399 . http://doi.org/10.1002/2016JC012426

Kudryavtsev Vladimir, Kozlov I., Chapron Bertrand, Johannessen J. A. (2014), Quad-polarization SAR features of ocean currents . Journal Of Geophysical Research-oceans , 119(9), 6046-6065

Kudryavtsev Vladimir, Myasoedov Alexander, Chapron Bertrand, Johannessen Johnny A., Collard Fabrice (2012), Imaging mesoscale upper ocean dynamics using synthetic aperture radar and optical data . Journal Of Geophysical Research-oceans , 117, http://doi.org/10.1029/2011JC007492

Rascle Nicolas, Nouguier Frederic, Chapron Bertrand, Mouche Alexis, Ponte Aurelien (2016), Surface roughness changes by fine scale current gradients: Properties at multiple azimuth view angles . Journal Of Physical Oceanography , 46(12), 3681-3694, http://doi.org/10.1175/JPO-D-15-0141.1

Rascle Nicolas, Chapron Bertrand, Ponte Aurelien, Ardhuin Fabrice, Klein Patrice (2014), Surface Roughness Imaging of Currents Shows Divergence and Strain in the Wind Direction, Journal Of Physical Oceanography , 44(8), 2153-2163

Kudryavtsev V, Akimov D, Johannessen Johnny, Chapron Bertrand (2005). On radar imaging of current features: 1. Model and comparison with observations - art. no. C07016 . Journal of Geophysical Union - Research C - Oceans , 110(C7), NIL_33-NIL_59

Johannessen J, Kudryavtsev V, Akimov D, Eldevik T, Winther N, Chapron Bertrand (2005). On radar imaging of current features: 2. Mesoscale eddy and current front detection - art. no. C07017 . JGR - Oceans , 110(C7), NIL_78-NIL_91

Plagge Amanda M., Vandemark Douglas, Chapron Bertrand (2012). Examining the Impact of Surface Currents on Satellite Scatterometer and Altimeter Ocean Winds . Journal Of Atmospheric And Oceanic Technology , 29(12), 1776-1793 .

Romeiser R., Thompson D. R., “Numerical study on the Along-Track Interferometric Radar Imaging Mechanism of Oceanic Surface Currents”, IEEE Trans. Geo. Rem. Sensing, Vol.38, No.1, January 2000.

Hansen M.W., Kudryavtsev V., Chapron B., Johannessen J.A., Collard F., Dagestad K.F., Mouche A.A., Remote Sensing of Environment, May 2012, Volume 120, Pages 113–122**,** http://dx.doi.org/10.1016/j.rse.2011.10.033

# 5. Forward and Retrieval Model Summary

A summary of key features of the forward and retrieval models is given in the table below.

| Models | Input Geophysical Parameters | | | | Surface Model Characteristics | | | | | | Output Ggeophysical Parameters | | | Input System Parameters | | |
|---|---|---|---|---|---|---|---|---|---|---|---|---|---|---|---|---|
| | Wind Vector | Current Vector | Wave Age | Spectral Model | Breaking waves | Lagrangian,+ Skewness | Electric Permitivity | Current Gradient | Rain rate | SST | NRCS | DCA | Image Cross Spectra | Inc. Angle | Polarization | Radar Freq. |
| Forward models - NRCS | yes | - | yes | Yes | Yes | Yes | Yes | No | No | No | Yes | | | Yes | Yes | Yes |
| Forward models - DCA | yes | yes | yes | Yes | Yes | Yes | Yes | No | No | No | | Yes | | Yes | Yes | Yes |
| Forward models - Spectra | yes | yes | yes | Yes | No | No | Yes | No | No | No | | | Yes | Yes | Yes | Yes |

| | Input Observed SAR Parameters | | | | Input Modelled SAR Parameter | | | Output Ggeophysical Parameters | | | Input System and Observation Errors | | |
|---|---|---|---|---|---|---|---|---|---|---|---|---|---|
| | NRCS | DCA | Image Cross Spectra | AUX-WIND | NRCS | DCA | Image Cross Spectra | Wind Vector | Current Vector | Wind Sea Hs | DCA variance | NRCS variance | Spectral Variance |
| Retrieval Model | Yes | Yes | Yes | Optional | Yes | Yes | Yes | Yes | yes | Optional | Yes | Yes | Yes |